RSC Advances

PAPER

View Article Online
View Journal | View Issue

Cite this: *RSC Adv.*, 2022, **12**, 15992

Photocatalytic hydrogen evolution over cyanine-sensitized Ag/TiO_2†

Layla Almazroai, *[a] Rasha E. El-Mekawy, [ab] Rihab Musa[c] and Lina Ali [c]

Sensitization of TiO_2 by dyes such as cyanine and their derivatives is used as a technique to improve potency for the production of hydrogen gas as an alternative green fuel. These dyes shift the spectrum of TiO_2 from the UV region to the visible region, enabling it to harvest as much sunlight as possible. Herein, four different derivatives of cyanine (labelled **C1**, **C2**, **C3**, and **C4**) were prepared and doped in Ag/TiO_2 *via* the impregnation method. The properties of the prepared photocatalysts were studied by XRD, SEM-EDS, FTIR, and UV-visible spectroscopy. The sensitized photocatalysts exhibited a similar morphology, nanoscale particle size, and good absorbance in the visible region. The rate constant for the photocatalytic activity of Ag/TiO_2 showed a great enhancement for hydrogen evolution after sensitization from 0.088 to 0.33 μmol min^{-1}. Doping of the **C2** derivative in Ag/TiO_2 promoted the photocatalytic and sonophotocatalytic rates of H_2 production by 7.5 and 9 times, respectively. Also, the amount of photocatalyst had a significant effect on the photocatalytic activity of the sensitized Ag/TiO_2, where 0.14 g was the optimum dose, giving the maximum yield at both the initial rate and 300 min. One of the important factors causing the efficiency to reach high levels is the inhibition of photogenerated electron/hole recombination. This was achieved by adding a small quantity of methanol, which increased the rate by 9 times. The stability of the prepared photocatalysts was tested, which gave good results even after their 5th use. All the results confirmed that the sensitization of metal oxides is a promising solution in industry to produce clean energy (H_2) in high quantities over highly stable photocatalysts.

Received 6th February 2022
Accepted 13th May 2022

DOI: 10.1039/d2ra00788f

rsc.li/rsc-advances

1. Introduction

Currently, significant efforts are devoted to research in the field of chemistry, particularly on the chemistry of light-sensitive compounds with biological and industrial importance. Specifically, this is meaningful in the field of organic chemistry and solar energy for applications such as photodynamic therapy,[1] nonlinear optics,[2] optical data storage,[3] laser materials[4,5] and solar and photovoltaic cells.[6,7] Therefore, the development of these compounds is important due to their photosensitivity, resulting from the excitation of electrons that are stimulated in the form of magnetic resonance. This is important for many vital applications. One of the most important types of compounds are cyanine dyes,[8–11] which have positive effects on photocatalytic activity (Fig. 1). Herein, a series of novel cyanine dyes was prepared and applied in the field of renewable energy.

Recently, H_2 fuel has become a hot topic as an effective renewable energy to replace fossil fuel and address pollution.[12,13] In this case, the large-scale use of photocatalysis for water splitting appears to be a rich source of hydrogen using various techniques.[14–16] Accordingly, to achieve this, metal oxide semiconductors show great potential due to their properties such as nontoxicity, corrosion resistance, abundance, low cost and photostability. Amongst the metal oxides, such as ZnO, Fe_2O_3 and SnO,[17–20] titanium dioxide (TiO_2) is considered one of

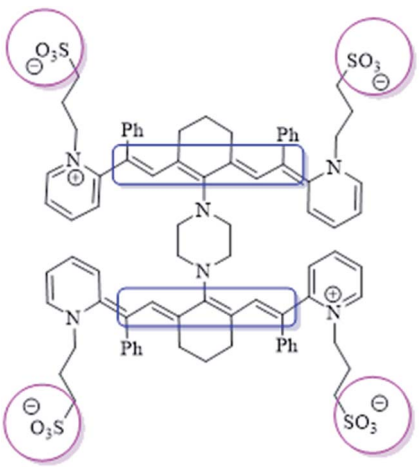

Fig. 1 Cyanine dye model.

[a]*Department of Chemistry, Faculty of Applied Science, Umm Al-Qura University, Makkah, Saudi Arabia. E-mail: lsmazroai@uqu.edu.sa*

[b]*Department of Petrochemicals, Egyptian Petroleum Research Institute, Nasr City, Cairo, Egypt*

[c]*Undergraduate students, Saudi Arabia*

† Electronic supplementary information (ESI) available. See https://doi.org/10.1039/d2ra00788f

the best semiconductors for this purpose.[21,22] However, despite the great advantages of TiO_2, there are some major drawbacks that reduce its photocatalytic efficiency such as wide band gap, which is approximately 3.2 eV, only allowing it to absorb UV irradiation, which accounts for 5% of solar energy. Also, the recombination of photoexcited electrons and holes is a big challenge in this case. These restraints have largely been overcome by modulating the composition of TiO_2 materials, such as through metal doping.[23,24] Novel metals have gained considerable attention due to their significant results in water splitting, which consequently increase the rate of hydrogen production.[25–28] Doping of TiO_2 with silver has been demonstrated in numerous studies as a way for enhancing the photocatalytic process.[29,30] The absorption spectrum of TiO_2 is shifted to the visible region in the presence of silver. Additionally, silver can inhibit the recombination of e^-/h^+ pairs by trapping the photogenerated electrons from the VB of TiO_2.[31,32] However, the desired industrial yield of photocatalytic H_2 production has not been reached to date, although different metal–metal oxides have been fabricated using several techniques. Therefore, TiO_2 still needs further improvements to make it more energy efficient. Alternatively, it is known that dyes with unique optical properties are used widely in many fields.[33,34] Accordingly, these dyes were introduced in the manufacture of solar cells (known as dye-sensitized solar cells, DSSCs) by Grätzel and O'Regan[35] more than twenty years ago. Dye-sensitized semiconductors as photocatalysts for the production of H_2 enhance the harvesting of solar light and may lead to a higher yield of H_2 production. Thus, the role of dyes as a photosensitizer has been studied in many works. For instance, fluorescein as a photosensitizer was added to an Ag/g-C_3N_4 composite and the H_2 evolution rate was 2014. 20 μmol g^{-1} h^{-1} h which was 4.8-times higher than that of 3 wt% Ag loaded on the same support.[36] Also, Pt–TiO_2 sensitized with a new thiophenothiazine-based dye produced approximately 1048 μmol of H_2 with a quite high quantum yield (50%).[37] In another study, an asymmetric zinc phthalocyanine derivative was used to sensitize TiO_2, expanding its absorption edge to 700 nm under monochromatic light irradiation with a quantum efficiency of 0.2%.[38] All these studies demonstrated that the dye-sensitization of semiconductors such as TiO_2 can enhance their photocatalytic activity in the water splitting process. Moreover, the processes for the photoexcitation of electrons are similar to that in DSSCs. Among the family of dyes, cyanine has attracted attention owing to its photophysical and photochemical properties. Cyanine compounds are distinguished by their broad absorbance in the UV-vis region, molar extinction coefficient, and Stokes shift.[39–42] Hence, cyanine dye is highly attractive for use in the field of H_2 energy. The design of photocatalysts is not the only factor affecting the H_2 evolution process, the structure of the photoreactor also has a significant impact on the production rate. In the last few years, an innovative technique has been utilized to improve the conversion efficiency. This technique is known as sonophotocatalysis, involving the coupling of ultrasound irradiation (sonolysis) with light irradiation (photolysis).[43,44] Ultrasound waves are characterized by the induction of cavitation phenomena. When water is irradiated by ultrasound waves, a localized hot spot is generated with a temperature reaching up to 5000 °C and pressure of 1000 bars. As a result of the cavitation process, water decomposes to hydrogen peroxide (H_2O_2), which plays a role in the formation of more reactive oxygen species during the photocatalytic reaction. Furthermore, the sonolysis process promotes mass transfer from the solid/liquid interface, maintains the active surface area of the catalyst by preventing its aggregation, and enhances the fast removal of H_2 from the bubbles. Consequently, ultrasound radiation combined with the photocatalysis process (sonophotocatalysis) promotes H_2 production.[45,46] In our previous work,[47] it was proven that the effect of sonophotocatalysis of dye-sensitized Cu–TiO_2 with a high absorption efficiency in the visible region for H_2 evolution was greater than *via* only photocatalysis by 7 times.

In this work, Ag was considered due to the above-mentioned reasons. Also, as it is well-known from the previous research that Ag as a noble metal has a high photoconversion yield as a result of its localized surface plasmon resonance,[48,49] and it also exhibits high antibacterial activity.[50] Furthermore, supported silver heterogeneous catalysis has been effectively used at the industrial scale as an oxidative agent to convert ethylene to ethylene oxide and methanol to formaldehyde.[51] Herein, the effect of sound waves and photoirradiation, catalyst dose, and presence of methanol was investigated to improve the hydrogen production efficiency of four new cyanine derivatives and sensitization of Ag/TiO_2. These dyes were chosen because of their characteristic spectral data, which are photosensitive due to their highly conjugated system. As the conjugation increases, the resonating structures and photosensitivity increase.

2. Results and discussion

2.1 Characterization of the cyanine derivatives

Based on previous studies and the introduction, our aim was to prepare a new series of photosensitive cyanine dyes that exhibit distinct and fruitful application effects in the field of renewable energy and can used as photocatalysts in energy applications (all ^{1}H-NMR and IR spectra are displayed in S1(a–h)).† Firstly, 3-((*Z*)-2-((*E*)-2-(2-chloro-3-((*E*)-2-phenyl-2-(1-(3-sulfonatopropyl) pyridin-1-ium-2-yl)vinyl) cyclohex-2-en-1-ylidene)-1-phenylethylidene)pyridin-1(2*H*)-yl)propane-1-sulfonate (**1**)[8] was reacted with (*E*)-4-((4-aminophenyl)diazinyl)-*N*,*N*-dimethylaniline (**2**) in basic medium in the presence of *N*,*N*-dimethylformamide as a solvent and sodium hydroxide pellets for 5 h under an inert atmosphere of nitrogen gas to remove air bubbles from the reaction media and protect the reaction from air, giving excellent yield of the target compound **3**. The poly-conjugated system of polymethine cyanine dye **3** was confirmed by IR spectroscopy, which showed a strong absorption band at $\ddot{v} = 3450$ cm^{-1} related to the NH group and absence of an absorption band at $\ddot{v} = 3443–3449$ cm^{-1} owing to two halves of NH_2 group. This indicates that the reaction successfully occurred. The ^{1}H NMR spectrum exhibited a singlet signal at $\delta = 10.23$ ppm, which is attributed to the NH proton. The mass spectrum of **3** exhibited the molecular ion peak at $m/z = 922$ (M^+, 52%), corresponding to the molecular formula $C_{52}H_{53}N_6O_6S_2$. When compound **1** was combined with the pyrrole structure, the replacement of the

chlorine atom at the meso position occurred by the nitrogen of the pyrrole structure by removing HCl in the presence of *N*,*N*-dimethylformamide as the solvent and sodium hydroxide pellets for 5 h under an inert atmosphere of nitrogen gas, yielding structure **4**. Compound **4** was tested by element and Bunsen tests, which gave negative results, confirming the disappearance of chlorine. The IR spectrum exhibited no absorption band at $\ddot{v} = 3452\ cm^{-1}$. This is considered evidence of the formation of compound **4**, as outlined in Scheme 1.

Alternatively, penta methine cyanine dye **5** (ref. 8) resulted in the excellent synthesis of pentamethine cyanine dye **6** through reaction with 4-chlorobenzaldehyde in basic medium in the presence of *N*,*N*-dimethylformamide as the solvent and sodium hydride as the base for 5 h under an inert atmosphere of nitrogen gas. The structure **6** of was elucidated based on its correct analytical and spectral data. Its IR spectrum revealed the characteristic strong absorption band of the carbonyl group at $\ddot{v} = 1728\ cm^{-1}$. Moreover, its ^1H NMR spectrum exhibited a singlet signal at $\delta = 10.03$ ppm due to the CHO proton and absence of a signal at $\delta = 10.51$ ppm owing to the disappearance of the NH proton. The mass spectrum of **6** showed the molecular ion peak at $m/z = 625$ (M^+, 31%) corresponding to the molecular formula of $C_{36}H_{33}N_2O_4SCl$, as shown in Scheme 2.

2.2. Photosensitization properties of novel series of cyanine dyes 3, 4, 5 and 6

Cyanine dyes have a long-conjugated chain system. This system increases their magnetic resonance, and thus their stability in space, and increased generation of electron currents as a result of the electronic excitation process from the ground state to the first excited state and then to the triplet excited state as a result of the generation of singlet oxygen species. This process increases with an increase in the conjugated system, which is responsible for the activity of dyes. This occurs when it they are exposed to a quantity of photons from an external light source or sunlight. We found that the compounds possessed an absorption wavelength following the order of **3**: $\lambda_{max} = 720$ >; **4**: $\lambda_{max} = 710$; **6**: $\lambda_{max} = 707$ and **5**: $\lambda_{max} = 700$ (Fig. 2 and Table 1).

X-ray diffraction (XRD) gave information regarding the crystallinity of the synthesized chromophoric structures, where among the, compound **5** exhibited the highest crystallinity, as displayed in Fig. S2.†

Successively, the stability of these dyes presented an opportunity to employ them effectively as photocatalysts. All the compounds exhibited excellent stability, as demonstrated by the thermal gravimetric analysis (TGA). Firstly, the loss of moisture occurred at the point of weight loss due to the removal of the substituent at the meso position at high temperature, which typically had no influence on the conjugated framework. This indicates the suitability of these compounds for application in the field of renewable energy, as outlined in Fig. S3.†

The framework of the synthesized dyes **3**, **4**, **5** and **6** was observed by scanning electron microscopy (SEM) (Fig. S4†). The presence of white sites in SEM images revealed that the surface morphology of these compounds has active sites and pores, which allow the delocalization of their π-system and generation of a current of electrons continuously.[52,53] Alternatively, the subsequent photosensitization of the chromophores aid in their excitation to the triplet excited state, leading to the continuous generation of singlet oxygen species.

Noticeably, the conjugated methine cyanine dyes were screened as photo- and sono-catalysts for the production of hydrogen. Compound **5** exhibited the highest activity due to the presence of a free nitrogen atom, which increased its flexibility

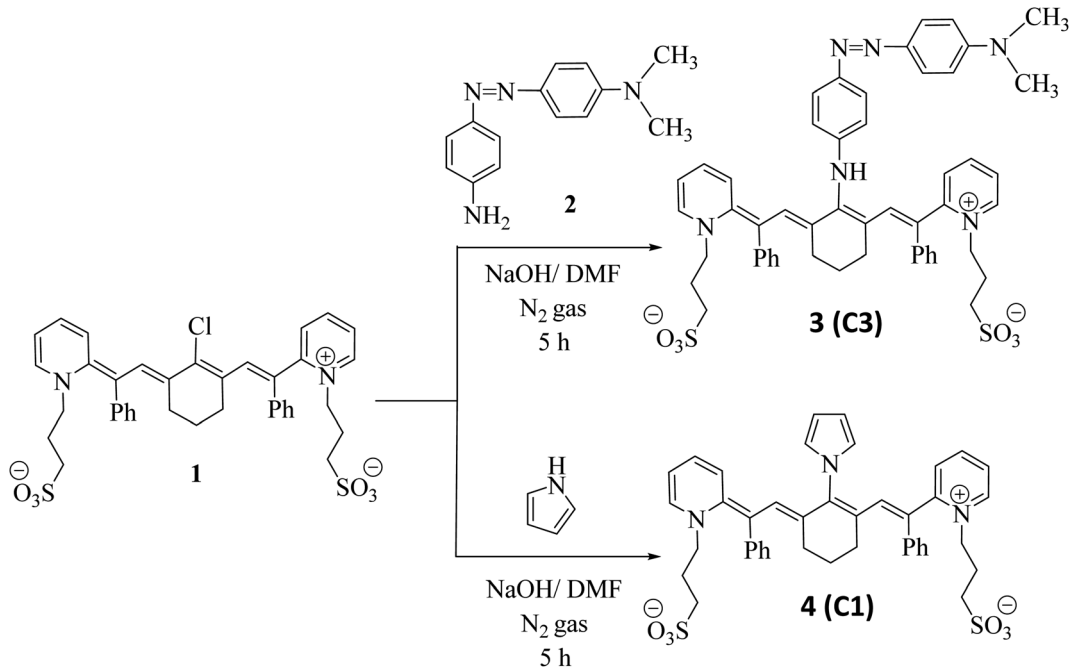

Scheme 1 Representative form of novel fruitful chromophoric heptamethine cyanine dyes 3 and 4.

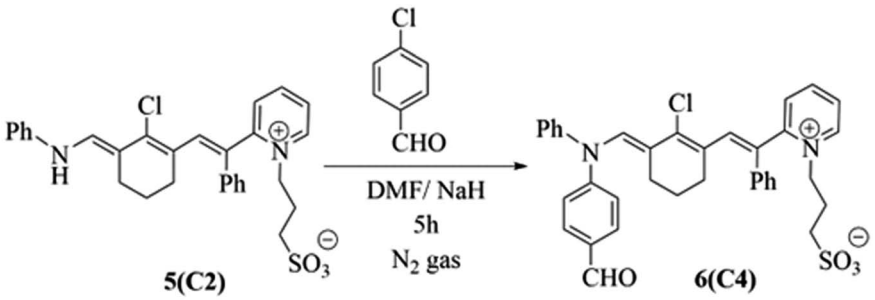

Scheme 2 Distinctive chromophoric photosensitizer **6**.

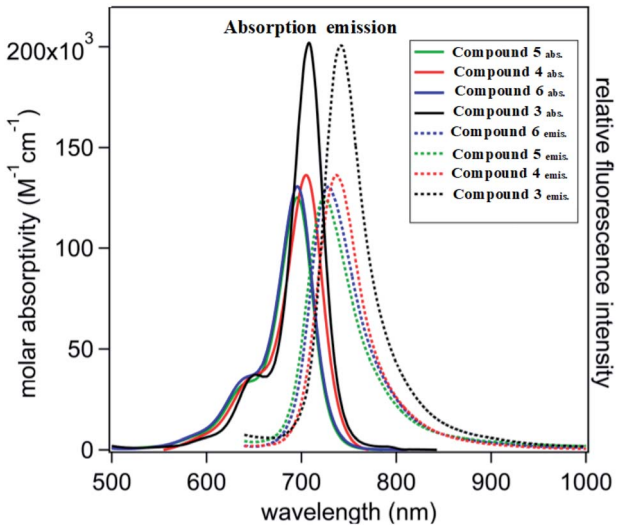

Fig. 2 Visible-near infrared (vis-NIR) normalized molar absorptivity (solid lines) and emission spectra (dotted lines).

and delocalization of its π-system, followed by compound **4** in reactivity owing to the presence of the pyrrole ring, which increased its conjugated system, and then photosensitization increased the generation of reactive oxygen species. The reactivity of the other compounds followed the order of **6** > **3** >**1**, where the carbonyl group of formyl in compound **6** increased its resonance and allowed its free rotation in space, compound **3** was slightly rigid, which is attributed to its azo group, and then the presence of chlorine in compound **1** decreased the active sites in its structure because of its electron-withdrawing nature rather than donating electrons to the system.

The prepared cyanine compounds were labelled after they were added to Ag/TiO_2 as follows: **C1(4)**, **C2(5)**, **C3(3)**, and **C4(6)**, respectively.

2.3. Characterization of sensitized Ag/TiO_2

2.3.1 XRD analysis. The crystallinity of the prepared samples and their particle size were determined by X-ray diffraction analysis (XRD). The XRD patterns of 1% Ag/TiO_2 and as-synthesized **C1**–Ag/TiO_2, **C2**–Ag/TiO_2, **C3**–Ag/TiO_2, and **C4**–Ag/TiO_2 samples are shown in Fig. S5.† The distinct peak of Ag was not observed, which is probably due to the high dispersion of Ag on the surface of TiO_2, as mentioned later in the EDS section, and its low concentration.[54,55] In some studies, when the silver doping was higher than 2 wt%, the XRD diffraction peaks of silver appeared at 38.1° and 64.5°,[54,56] but in this work, the content of Ag was 1 wt%. The XRD peaks of Ag/TiO_2 and all the **C(1–4)**–Ag/TiO_2 samples represented TiO_2 as the anatase phase, which is in agreement with the standard anatase peaks (JCPDS 78-2486). The rutile phase was not observed, which may be due to several reasons. When the Ag content range is less than 1.5%, it may stimulate the crystallization of the rutile phase to anatase phase. In addition, it was clear that the intensity of the anatase peaks representing 85% of TiO_2 P25 was quite low. This may have caused the rutile peaks to not be visible. Also, the parameters of the analysis could be a reason for the low intensities.

The particle sizes of the crystalline photocatalysts were calculated through the Scherrer equation. Table S1† displays a variety of large nanoscale particle sizes for the synthesized Ag/TiO_2 and **C(1–4)**–Ag/TiO_2 due to the bulky organic structure of the cyanine derivatives. Additionally, based on the geometry, chemical composition, and structure of the cyanine derivative dyes, the agglomeration of the particles may increase after dye sensitization. Also, there is a relation between the agglomeration process and the anchoring groups (*e.g.*, –COOH and –SO_3H). Nevertheless, introducing chlorine in the dye structure decreased the active sites in the structure because of its electron-withdrawing nature. Accordingly, in **C4** with a particle size of 71.1 nm, despite the presence of Cl^-, the introduction of carbonyl acid as an anchoring group in the dye structure led to the formation of an ester linkage. Also, the amino group in **C2** (94.4 nm) increased its particle size (delocalization of π electrons). **C3** had the largest particle size (104.6 nm), which can be explained by the introduction of the rigid aromatic unit (azo group) over the π-conjugated bridge.

2.3.2 SEM/EDX analysis. The study of the surface morphology and elemental composition of pure Ag/TiO_2 and the cyanine-sensitized Ag/TiO_2 photocatalysts was performed through SEM and EDX, respectively. Fig. 3(A and B) illustrate the SEM micrographs of the photocatalysts before and after sensitization with an average size of 108.77 nm and 105.72 nm, respectively. They have a nearly spherical shape with nanoscale particles as a result of the modification of TiO_2 with silver.[57] Fig. 3B displays slight particle agglomeration owing to the

Table 1 Absorption spectroscopy features of the synthesized polymethine cyanine dyes **3**, **4**, **5** and **6**

Compound no.	Absorption bands λ_{max} (nm)	Emission bands λ_{em} (nm)	Molar absorptivity log ε (L mol^{-1} cm^{-1})	Stoke shift $\lambda_{max} - \lambda_{em}$	(Quantum yield) Q
3	720	760	5.31	40	1.055
4	710	740	5.11	30	1.042
5	700	720	5.07	20	1.028
6	707	739	5.09	32	1.045

sensitization of Ag/TiO_2 with the cyanine dye derivatives. Alternatively, the EDX elemental analysis of the sensitized **C(1–4)**–Ag/TiO_2, as shown in Fig. 7C, detected the presence of O, Ag, Ti and C as the main constituents. The presence of carbon indicates the successful cyanine sensitization of Ag/TiO_2. Moreover, the elemental analysis clearly showed the highly uniform distribution of the silver and dye on the surface of TiO_2. Thus, the obtained results confirm the excellent preparation of these photocatalysts.

2.3.3 FTIR analysis. Fig. S6† illustrates the FTIR spectra of the pure and the sensitized Ag/TiO_2 to investigate the strong attachment between the Ag/TiO_2 surface and the dye molecules. The FTIR analysis was recorded in the range of 4000–300 cm^{-1}. The broad peak at ~3441 cm^{-1} is assigned to the hydroxyl group stretching vibration mode (O–H bending) of the titanium dioxide surface and the band at ~1631 cm^{-1} is associated with the O–H bending vibration, which indicate the adsorption of water molecules or moisture in the samples.[58,59] The strong broad bands in the range of 675–512 cm^{-1} confirm the presence of metal oxygen bonding, which can be attributed to the bridging stretching and stretching modes of Ti–O–Ti, Ti–O, Ag–O–Ti and Ag–O.[60] The peak at 1382 cm^{-1} for **C3**–Ag/TiO_2 is ascribed to the C–H stretching of the alkyl group responsible for the attachment between **C3** and the Ag/TiO_2 surface, resulting in an increase in the photocatalytic activity of **C3**–Ag/TiO_2. Meanwhile, the peak at ~2900 cm^{-1} corresponds to the C–H stretching vibration for the aldehyde group of **C4**–Ag/TiO_2.

2.3.4 Optical properties. The main goal of adding metals is to exploit the collection of visible light as much as possible, which represents around 40% of sunlight. Fig. 4 demonstrates the positive effect of incorporating of Ag in the TiO_2 lattice by the shifting its spectrum toward the visible region. However, its absorbance is still not at the desired level. Thus, the idea of modification of photocatalysts concerning an enhancement in optical properties by sensitizing them by a dye is logical. As shown in Fig. 4, the absorbance peaks of the sensitized Ag/TiO_2 photocatalysts in the visible region were more intense and broad owing to their conjugated double bonds.

3. Study of the activity of the prepared photocatalysts for hydrogen production

3.1 Photo- and sonophotocatalytic hydrogen production

The effect of these dyes, which harvest more energy in the visible region, on the hydrogen evolution activity was as

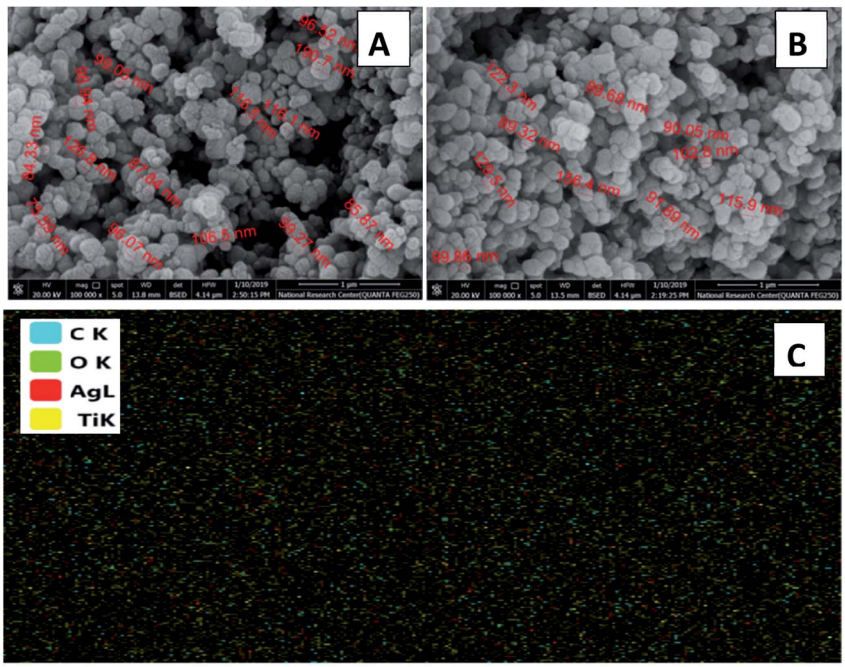

Fig. 3 SEM images of Ag/TiO_2 (A) before and (B) after sensitization and (C) EDX mapping of sensitized Ag/TiO_2.

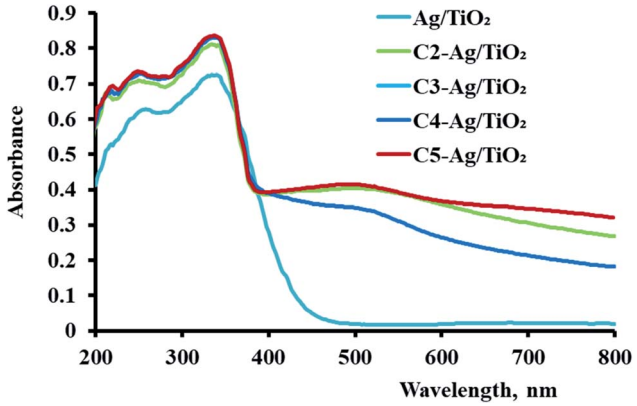

Fig. 4 Optical spectra of Ag/TiO_2 and the sensitized Ag/TiO_2 samples.

expected. As shown in Fig. 5(A), all the derivatives of cyanine loaded on Ag/TiO_2 were more effective (3.5–6 times) than that without them. Furthermore, in the case of sonophotocatalysis, as shown in Fig. 5(B), the activity increased by 5–7.5 times. Moreover, the rate constant of the photocatalytic and sonophotocatalytic hydrogen evolution over Ag/TiO_2 was 0.088 and 0.33 μmol min^{-1}, respectively. The presence of cyanine derivatives promoted the photocatalytic rate to 0.39–0.55 μmol min^{-1} and 1.95–3.3 μmol min^{-1} in the case of the addition of acoustic radiation to the photocatalysis process. The extent of the formation electron/hole pairs, which are the main reactive species in this process, depends on the ability of the photocatalyst to absorb more energy from light and the lifetime of these species. Thus, the structure of dyes molecules causes them to play a main role in the formation of more reactive pairs, as displayed in Fig. 4, which proved this effect concerning the ability of absorption.

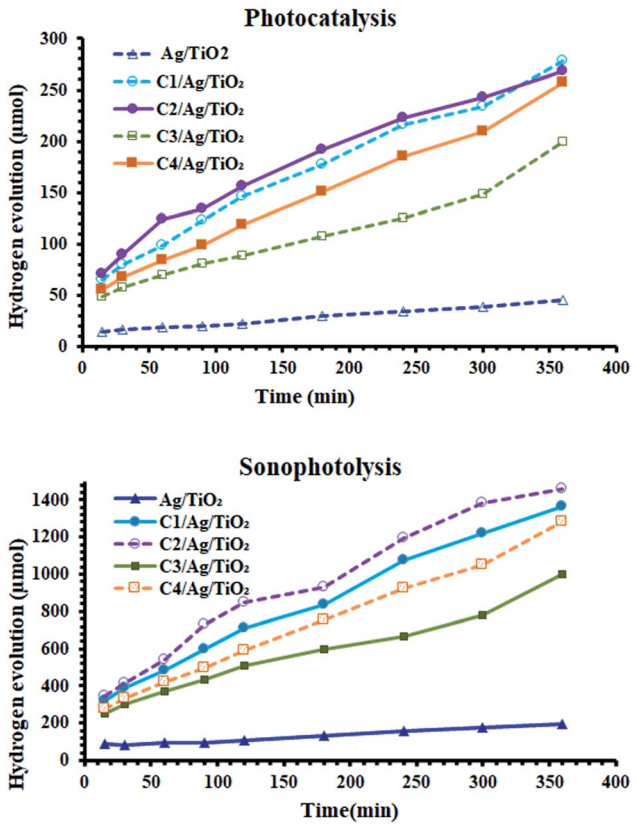

Fig. 5 (A) Photocatalytic activity and (B) sonophotocatalytic activity of the prepared sample before and after the sensitization of Ag/TiO_2.

According to the comparison of sono- and photocatalysis, the activity of the derivatives of cyanine were somewhat different. Their activity in photocatalytic hydrogen production followed the order of **C2** > **C1** > **C4** > **C3**, noting that the behavior of **C1** and **C2** in photocatalysis were nearly similar. This varying effect of their activities is due to the structure of these dyes and their properties in the sensitized Ag/TiO_2 for the production of the alternative fuel. The characterization studies mentioned previously are consistent with the activity of the sensitized photocatalysis. The higher absorbance, uniform distribution and the particles size can be correlated with the positive effect of these samples in this process. **C3** exhibited the lowest activity because it had the lowest absorbance intensity and largest particle size.

Alternatively, Fig. 6 demonstrates the synergistic effect on the amount of hydrogen evolved. By sonophotoirradiation of the photocatalyst, the amount of hydrogen produced was larger than that by only photoirradiation by 5.7 times after 5 h. During the heterogeneous reaction, the aggregation of small particles is very probable. The agglomeration of particles is one of the reasons for the reduction in the activity of catalysts in heterogeneous processes, lowering their surface area. Accordingly, sound waves are a physical force that inhibits the aggregation of nanoparticles. Additionally, the waves may contribute to the formation of more photogenerated reactive pairs (electron/hole), which yields higher activity.

3.2 Effect of catalyst dose

Because of the dependence of photocatalysis on the formation of photogenerated species on the surface of the catalyst, the number of illuminated particles should be considered. Fig. S7†

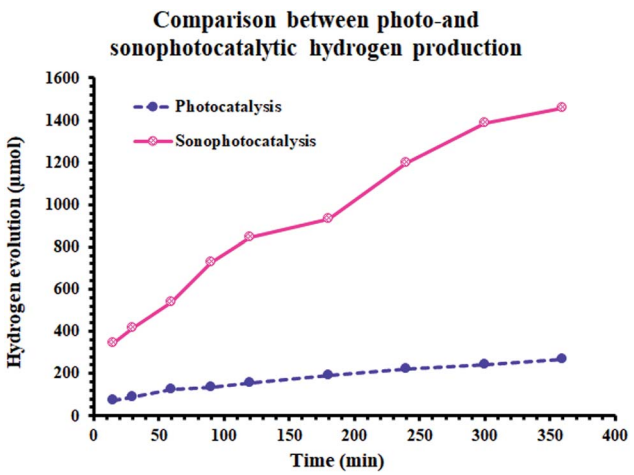

Fig. 6 Comparison between photo- and sonophotocatalytic hydrogen production.

clearly displays the effect of the catalyst dose. The optimum dose was 0.14 g, after which the hydrogen production decreased. This result is in agreement with many previous studies.[61,62] Excess particles over the optimum dose shields other particles from the light source. In addition, a large dose may result in more agglomeration, which inhibits the activity of photocatalyst. The behavior of the different particle sizes initially and after 5 h was similar.

3.3 The effect of methanol as a sacrificial agent

The production of hydrogen gas from pure water is an uphill reaction ($\Delta H = 286$ kJ mol^{-1}). Thus, the addition of small quantities of a sacrificial reagent such as methanol is considered one of the ways to promote the efficiency of hydrogen production significantly, as obtained herein and in most previous studies.[63] Fig. S8† shows the obvious effect of methanol molecules in enhancing of the amount of hydrogen produced over **C2**/Ag/TiO_2. A small amount of methanol (200 μL) was sufficient to increase the rate by 9 times, which indicates to the importance of the presence of small organic molecules. Methanol acts as an electron donor and is oxidized by the photogenerated hole ($^{\bullet}OH$) formed at the HOMO of the dye molecule or VB of TiO_2 (lower probability). The reaction between methanol and the photogenerated hole may produce reactive oxidative radicals, which achieve one-half reaction of water splitting. This indicated that the role of methanol is to produce an electron donor, injecting its electrons to the conduction band or LUMO of the dye.[63–65] The following equations were suggested for the oxidation of methanol by Chen *et al.*:[63]

$$H_2O\ (l) + h^+ \rightarrow {}^{\bullet}OH + H^+ \quad (1)$$

$$CH_3OH\ (l) + {}^{\bullet}OH \rightarrow {}^{\bullet}CH_2OH + H_2O \quad (2)$$

$${}^{\bullet}CH_2OH \rightarrow HCHO\ (l) + H^+ + e^- \quad (3)$$

After a series of steps, the final products are CO_2 and H_2O.

3.4 The mechanism of the photocatalytic hydrogen production

The mechanism for the photoactivity of the sensitized TiO_2 with some additives such as silver and methanol or the synergistic action using sound waves has been suggested in many studies,[66–69] summarized Fig. 7. Considering that the results of this study are consistent with the previous studies, it is possible to predict the mechanism. The first step in any photocatalytic reaction is photoexcitation by light. The Xe lamp used mimic the sunlight, in which UV radiation represents about 4%. According to this, it is reasonable that the light absorption by the dye molecule would be the more probable as the first step than the photoexcitation of TiO_2.[70] After photoexcitation, the excited electrons transfer from the LUMO state of the dye to the CB of TiO_2, which has a lower energy than the excited level of cyanine.[71] The photocurrent analysis in similar studies confirmed that the resistance of electron transfer plays a role in the generation and accumulation of charge carriers. According

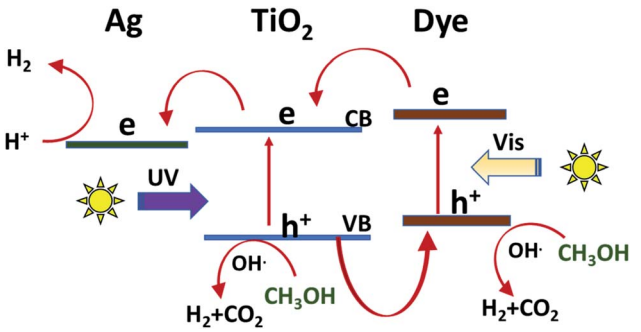

Fig. 7 Suggested mechanism for the photocatalytic production of hydrogen over the sensitized Ag/TiO_2.

to these results, it is expected that the resistance of the dye-sensitized TiO_2 is the lowest and the charge transfer is the fastest, and therefore the probability of the recombination of charge carriers would be the lowest in **C2**/Ag/TiO_2, as displayed by the photocatalytic hydrogen production.[72,73] Additionally, the four prepared cyanine sensitized photocatalysts may differ in incident photo-to-electric conversion efficiency (IPECE), which may act as an indicator of the rate of the back reaction between injected electrons and the excited state of the dye.[71]

Silver as noble metal nanoparticles can act as photo-generated electron trapping sites, and then reduce the electron–hole recombination compared with the bare TiO_2, the absorption of Ag/TiO_2 shifted to a longer wavelength (towards the visible region) due to the localized surface plasmon resonance (LSPR) of the Ag NPs. Alternatively, SPR effect can promote the generation of charge carriers in the photocatalyst by increasing the local electric field near metal nanoparticles.[74–76]

3.5 The reusability of sensitized Ag/TiO_2

Among the factors that should be considered in industry for photocatalytic fuel production is the maintained activity for many uses. The catalyst reusability process was investigated for five cycles. Specifically, 0.1 g of **C2**/Ag/TiO_2 in 100 mL of deionized water and 8 mM methanol were irradiated for 60 min. Subsequently, the photocatalyst was separated, dried, and reused. The prepared sensitized photocatalysts demonstrated ability to be active for 5 cycles, as shown in Fig. 8. The activity of **C2**/Ag/TiO_2 decreased by only 6% after the fifth use, which is ascribed to the loss of some materials during treatment and/or aggregation during the reaction.[77,78] However, the low loss (6%) makes these photocatalysts valuable due their stability and lack of tendency to adsorb the reaction products, allowing their further use.

4. Experimental

4.1. Preparation of various cyanine dyes

4.1.1 3-(2-((*E*)-1-Phenyl-2-((*E*)-2-(4-((*E*)-2-((*E*)-2-phenyl-2-(1-(3-sulfonatopropyl)pyridin-1-ium-2-yl)vinyl)-6-((*Z*)-2-phenyl-2-(1-(3-sulfonatopropyl)pyridin-2(1*H*)-ylidene)ethylidene)cyclohex-1-en-1-yl)piperazin-1-yl)-3-((*Z*)-2-phenyl-2-(1-(3-

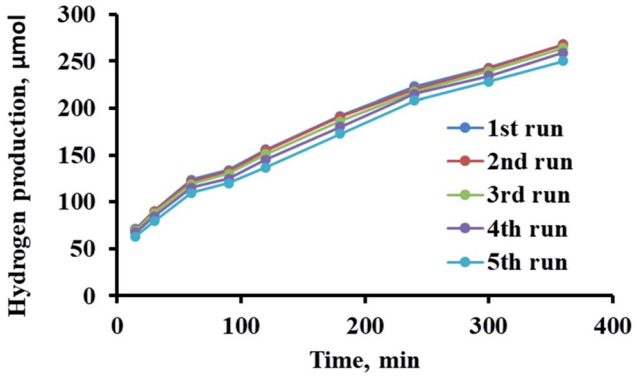

Fig. 8 Reusability of C2/Ag/TiO_2 for 5 cycles.

sulfonatopropyl)pyridin-2(1*H*)-ylidene)ethylidene)cyclohex-1-en-1-yl)vinyl)pyridin-1-ium-1-yl)propane-1-sulfonate (3). Under nitrogen gas, a mixture of (0.01 mol) of compound **1** and 0.01 mol of *E*−4-((4-aminophenyl) diazinyl)-*N*,*N*-dimethylaniline (**2**) was refluxed in a two-neck round-bottomed flask fitted with an air condenser in *N*,*N*-dimethylformamide and anhydrous sodium hydroxide (0.025 mol) for 5 h. The reaction was left to cool overnight, and then poured into ice-cooled water and was acidified by diluted HCl. The isolated solid was filtered and purified by column chromatography using CH_2Cl_2 : hexane (3 : 1), resulting in the formation of compound **3**.

Yield 92%; red crystals; m.p. 219 °C; IR (KBr): ύ/cm^{-1} = 3450 (NH), 3093 (Ar-H), 2924 (CH_2), 1667 (C=N), 1598 (C=C); ^{1}H NMR (DMSO-d_6) δ/ppm = 1.38 (m, 2H, **C5**–H_2 of cyclohexenyl ring), 2.93 (t, 4H, **C4**–H_2 and **C6**–H_2 of cyclohexenyl ring), 3.17–3.61 (m, 6H, 2 CH_2–SO_3, CH_2–N), 4.05 (t, 2H, CH_2–N^+), 5.26 (s, 1H, =CH), 6.12 (s, 1H, =CH), 6.60–8.74 (m, 26H, Ar-H, pyridine-H and pyridinium-H, two benzene rings), 10.23 (s, 1H, NH); ^{13}C NMR (DMSO-d_6) δ/ppm = 21.0, 30.6, 41.3, 101.8, 111.7, 112.4, 114.6, 121.1, 122.4, 125.0, 127.2, 127.9, 128.6, 136.6, 137.3, 144.4, 145.8.; MS: (*m*/*z*, %) 921 (M^+, 95%), 841 (34%), 761 (25%), 719 (54%), 677 (60%), 633 (39%), 556 (26%), 528 (100%), 451 (53%), 437 (45%), 360 (40%); anal. calcd for $C_{52}H_{53}N_6O_6S_2^-$ (921): C, 67.75%; H, 5.75%; N, 9.12%. Found: C, 67.74%; H, 5.74%; N, 9.10%.

4.1.2. 3-(2-((*E*)-1-Phenyl-2-((*E*)-3-((*Z*)-2-phenyl-2-(1-(3-sulfonatopropyl)pyridin-2(1*H*)-ylidene)ethylidene)-2-(1*H*-pyrrol-1-yl)cyclohex-1-en-1-yl)vinyl)pyridin-1-ium-1-yl)propane-1-sulfonate (4). Under nitrogen gas, a mixture of (0.01 mol) of compound **1** and 0.01 mol of pyrrole was refluxed in a two-neck round-bottomed flask fitted with an air condenser in *N*,*N*-dimethylformamide and anhydrous sodium hydroxide (0.025 mol) for 5 h. The reaction was left to cool overnight, and then poured into ice-cooled water and acidified with dil. HCl. The isolated solid was filtered and purified by column chromatography using CH_2Cl_2 : hexane (3 : 1), resulting in the formation of compound **4**.

Yield 85%; reddish brown crystals; m.p. 219 °C; IR (KBr): ύ/cm^{-1} = 3230 (Ar-H), 2924 (CH_2), 1583 (C=N), 1536 (C=C); ^{1}H NMR (DMSO-d_6) δ/ppm = 1.63 (m, 2H, **C5**–H_2 of cyclohexenyl ring), 2.33 (t, 4H, **C4**–H_2 and **C6**–H_2 of cyclohexenyl ring), 2.34 (m, 6H, 2 CH_2–SO_3, CH_2–N), 2.49 (t, 2H, CH_2–N^+), 4.04 (d, 2H, 2 = CH), 4.17 (d, 2H, 2 =CH), 6.30 (s, 1H, =CH), 6.60 (s, 1H, = CH), 6.94–7.74 (m, 18H, Ar-H, pyridine-H and pyridinium-H, two benzene rings); ^{13}C NMR (DMSO-d_6) δ/ppm = 11.0, 21.0, 30.6, 101.8, 112.4, 115.9, 116.1, 121.1, 122.3, 122.4, 127.2, 127.9, 128.6, 136.6, 137.3, 144.6, 147.1; MS: (*m*/*z*, %) 748 (M^+, 71%), 686 (24%), 607 (31%), 527 (21%), 447 (57%), 411 (19%), 375 (82%), 298 (71%), 221 (63%), 150 (53%); anal. calcd for $C_{42}H_{42}N_3O_6S_2^-$ (748): C, 67.37%; H, 5.61%; N, 5.61%. Found: C, 67.36%; H, 5.60%; N, 5.60%.

4.1.3. 3-(2-((*E*)-2-((*E*)-2-Chloro-3-(((4-formylphenyl)(phenyl)amino)methylene)cyclohex-1-en-1-yl)-1-phenylvinyl)pyridin-1-ium-1-yl)propane-1-sulfonate (6). Under nitrogen gas, a mixture of 0.01 mol of compound **5** and 0.01 mol of 4-chlorobenzaldehyde was refluxed in a two-neck round-bottom flask fitted with an air condenser in *N*,*N*-dimethylformamide and anhydrous sodium hydride (0.025 mol) for 5 h. The reaction was left to cool overnight, and then poured into ice-cooled water and acidified with dil. HCl. The isolated solid was filtered and purified by column chromatography using NH_2OH : CH_2Cl_2- : hexane (0.5 : 3 : 1), resulting in the formation of compound **4**.

Yield 67%; red crystals; m.p. 219 °C; IR (KBr): ύ/cm^{-1} = 3230 (Ar-H), 2924 (CH_2), 1583 (C=N), 1536 (C=C); ^{1}H NMR (DMSO-d_6) δ/ppm = 1.63 (m, 2H, **C5**–H_2 of cyclohexenyl ring), 2.34 (t, 4H, **C4**–H_2 and **C6**–H_2 of cyclohexenyl ring), 2.49 (t, 2H, CH_2–SO_3), 4.19 (t, 2H, CH_2–N^+), 6.32 (s, 1H, =CH), 6.63 (s, 1H, =CH), 6.94-7.74 (m, 19H, 3 Ar-H and pyridinium-H); ^{13}C NMR (DMSO-d_6) δ/ppm = 29.7, 119.6, 121.6, 121.9, 126.4, 127.0, 127.1, 127.2, 127.9, 128.6,129.6, 140.0, 145.8, 147.1; MS: (*m*/*z*, %) 624 (M^+, 54%), 595 (62%), 519 (51%), 505 (21%), 428 (25%), 348 (29%), 312 (62%), 298 (71%), 239 (100%), 162 (83%); anal. calcd for $C_{36}H_{33}ClN_2O_4S$ (624): C, 67.37%; H, 5.61%; N, 5.61%. Found: C, 67.36%; H, 5.60%; N, 5.60%.

4.2. Preparation of the sensitized Ag/TiO_2

1% Ag/TiO_2 was prepared as mentioned in our previous work *via* the wetness-impregnation method. A paste of Ag/TiO_2 was made by adding an appropriate amount of $AgNO_3$ solution gradually to TiO_2 powder (Degussa P25). The paste was dried, and then calcined at 500 °C for 2 h. For the preparation of the cyanine-sensitized Ag/TiO_2, 0.5 g of this sample was vigorously stirred in each cyanine derivative solution (1% w/v) for 24 h in the dark to ensure the complete adsorption of the dye on the surface of Ag/TiO_2. The prepared sensitized photocatalysts were centrifuged, washed with ethanol, washed with deionized water three times, and dried for 24 h.

4.3. Characterization

The melting point of the various cyanine dyes was measured using a Gallenkamp electric melting point instrument. Infrared (IR) spectra were measured (KBr disk) on a Mattson 5000 FTIR spectrometer, ^{1}H-NMR and ^{13}C NMR spectra were measured on a Bruker WPSY 200 MHz spectrometer with TMS as the internal standard and the chemical shifts are reported in δ ppm using DMSO-d_6 and/or $CDCl_3$ as the solvents at the Faculty of Science, Mansoura University, Egypt. Mass spectroscopy was performed

at 70 eV with a Varian MAT 311 and elemental analyses (C, H and N) were performed at the Microanalytical Center, Faculty of Science, Cairo University. The results were consistent (±0.03) with the theoretical values. X-ray Diffraction (XRD) was employed to determine the crystallinity of the polymer. X-ray diffraction was performed using a Philips PW 3710 (Philips, USA) diffractometer with CuKα radiation (λ = 0.1542 nm) in a sealed tube at 40 kV and 30 mA. Energy dispersive X-ray spectroscopy (EDS) and scanning electron microscopy (SEM) were performed using a Philips XL 30CP, USA. The films were cut and mounted on a brass stub with double-sided adhesive tape and coated with 50 Å of gold with an SCD-040 Balzers sputter coater. The specimen was finally characterized by SEM at accelerating voltage of 30 kV and at 7500, 10 000 and 15 000× magnification of the original specimen size.

The prepared sensitized Ag/TiO_2 was also characterized using the same instruments as mentioned in the characterization of the cyanine compounds.

4.4. Study of the photocatalytic and sonophotocatalytic activity of the prepared sensitized Ag/TiO_2

The hydrogen evolution was measured by withdrawing aliquots every 30 min from the irradiated mixture of 0.1 g sample dispersed in 100 mL of water and 0.2 mL of methanol. A 500 W Xe lamp was used in this study. The samples were analyzed by gas chromatography (Agilent GC 78900A) with a thermal conductivity detector (TCD) using argon as the carrier gas, and then the hydrogen gas was precisely detected. For the sonophotocatalytic study, a sonicator (20 kHz, 1800 W) with a Ti probe (20 mm) was used and immersed in the mixture to transfer ultrasound waves from the generator to the suspension irradiated by a Xe lamp simultaneously.

5. Conclusion

The photocatalytic hydrogen production was promoted significantly on the different derivatives of cyanine-sensitized Ag/TiO_2. However, the **C2**-sensitized Ag/TiO_2 had the highest photocatalytic activity in both photocatalysis (7.5 times) and sonophotocatalysis (9 times) compared with the unsensitized Ag/TiO_2. The optimum dose of the photocatalyst was 0.14 g, as expected according to many similar studies, which means that this small quantity of photocatalyst may give reasonable results. Additionally, a small amount of methanol promoted the photocatalytic activity of the sensitized photocatalysts by 9 times. The role of these molecules in photocatalytic hydrogen production is the inhibition of electron/hole recombination by consuming the generated holes. Therefore, the oxidation of methanol molecules over the surface of the photocatalyst resulting in the formation of more hydrogen gas. Besides, the study of the stability of the prepared photocatalysts is important economically, and this study confirmed their stability even after 5 uses. Ag/TiO_2 with the four different cyanine derivatives exhibited a similar effect, while all of them gave a higher yield of H_2 than the unsensitized Ag/TiO_2.

Conflicts of interest

The authors announce that there is no conflict of interest.

Acknowledgements

The authors are deeply grateful to the Deanship of Scientific Research at Umm Al-Qura University, which supported this work financially (Grant no 15SCI-3-3-0024).

References

1 J. Burschka, N. Pellet, S.-J. Moon, R. Humphry-Baker, P. Gao, M. K. Nazeeruddin and M. Grätzel, *Nature*, 2013, **499**, 316–319.
2 A. Levitz, F. Marmarchi and M. Henary, *Molecules*, 2018, **23**(2), 226.
3 T. L. Dost, M. T. Gressel and M. Henary, *Anal. Chem. Insights*, 2017, **12**, 1–6.
4 X. Liu, Z. Xu and J. M. Cole, *J. Phys. Chem. C*, 2013, **117**, 16584–16595.
5 C. P. Toseland, *J. Chem. Biol.*, 2013, **6**, 85–95.
6 A. A. Kostyukov, A. E. Egorov, M. G. Mestergazi, A. M. Shmykova, T. A. Podrugina, I. E. Borissevitch, A. A. Shtil and V. A. Kuzmin, *Mendeleev Commun.*, 2020, **30**, 442–444.
7 V. K. Saarnio, K. Salorinne, V. P. Ruokolainen, J. R. Nilsson, T.-R. Tero, S. Oikarinen, L. M. Wilhelmsson, T. M. Lahtinen and V. S. Marjomäki, *Dyes Pigm.*, 2020, **177**, 108282.
8 L. S. Almazroai and R. E. El-Mekawy, *RSC Adv.*, 2019, **9**, 24670–24681.
9 R. E. El-Mekawy and A. A. Fadda, *Bioorg. Med. Chem. Lett.*, 2018, **28**, 1747–1752.
10 R. E. El-Mekawy and A. A. Fadda, *RSC Adv.*, 2017, **7**, 54706–54716.
11 A. A. Fadda and R. E. El-Mekawy, *Dyes Pigm.*, 2013, **99**, 512–519.
12 S. Ban, W. Lin and J. Luo, *Int. J. Hydrogen Energy*, 2019, **44**, 1466–1473.
13 L. Hu, B. Zheng, Z. Lai and K. Huang, *Int. J. Hydrogen Energy*, 2014, **39**, 20031–20037.
14 M. Y. Ghaly, T. S. Jamil, I. E. El-Seesy, E. R. Souaya and R. A. Nasr, *Chem. Eng. J.*, 2011, **168**, 446–454.
15 J. Yu, Z. Chen, L. Zeng, Y. Ma, Z. Feng, Y. Wu, H. Lin, L. Zhao and Y. He, *Sol. Energy Mater. Sol. Cells*, 2018, **179**, 45–56.
16 P. Chen, P. Xing, Z. Chen, H. Lin and Y. He, *Int. J. Hydrogen Energy*, 2018, **43**, 19984–19989.
17 T. Wei, Y. N. Zhu, X. An, L. M. Liu, X. Cao, H. Liu and J. Qu, *ACS Catal.*, 2019, **9**, 8346–8354.
18 V. Vaiano, C. A. Jaramillo-Paez, M. Matarangolo, J. A. Navío and M. del Carmen Hidalgo, *Mater. Res. Bull.*, 2019, **112**, 251–260.
19 M. Navarrete, S. Cipagauta-Díaz and R. Gómez, *J. Chem. Technol. Biotechnol.*, 2019, **94**, 3457–3465.
20 C. Castañeda, F. Tzompantzi, A. Rodríguez-Rodríguez, M. Sánchez-Dominguez and R. Gómez, *J. Chem. Technol. Biotechnol.*, 2018, **93**, 1113–1120.

21 E. Wierzbicka, X. Zhou, N. Denisov, J. E. Yoo, D. Fehn, N. Liu, K. Meyer and P. Schmuki, *ChemSusChem*, 2019, **12**, 1900–1905.
22 A. A. Nada, W. M. A. El Rouby, M. F. Bekheet, M. Antuch, M. Weber, P. Miele, R. Viter, S. Roualdes, P. Millet and M. Bechelany, *Appl. Surf. Sci.*, 2020, **505**, 144419.
23 N. D. Phu, L. H. Hoang, P. Van Hai, T. Q. Huy, X. B. Chen and W. C. Chou, *J. Alloys Compd.*, 2020, **824**, 153914.
24 S. Wageh, L. S. Almazroai, A. Alshahrie and A. A. Al-Ghamdi, *J. Nanosci. Nanotechnol.*, 2018, **18**, 7682–7690.
25 G. Gong, Y. Liu, B. Mao, L. Tan, Y. Yang and W. Shi, *Appl. Catal., B*, 2017, **216**, 11–19.
26 E. Hussain, I. Majeed, M. A. Nadaem, A. Badshah, Y. Chen, M. A. Nadeem and R. Jin, *J. Phys. Chem. C*, 2016, **120**, 17205–17213.
27 O. Rosseler, M. V. Shankar, M. K. Le Du, L. Schmidlin, N. Keller and V. Keller, *J. Catal.*, 2010, **269**, 179–190.
28 E. Hussain, I. Majeed, M. A. Nadeem, A. Iqbal, Y. Chen, M. Choucair, R. Jin and M. A. Nadeem, *J. Environ. Chem. Eng.*, 2019, **7**, 102729.
29 C. Suwanchawalit, S. Wongnawa, P. Sriprang and P. Meanha, *Ceram. Int.*, 2012, **38**, 5201–5207.
30 X. F. Lei, X. X. Xue and H. Yang, *Appl. Surf. Sci.*, 2014, **321**, 396–403.
31 Y. K. Park, B. J. Kim, S. Jeong, K. J. Jeon, K. H. Chung and S. C. Jung, *Environ. Res.*, 2020, **188**, 109630.
32 S. Mohammed Harshulkhan, K. Janaki, G. Velraj, R. Sakthi Ganapthy and M. Nagarajan, *J. Mater. Sci.: Mater. Electron.*, 2016, **27**, 4744–4751.
33 A. Sułek, B. Pucelik, J. Kuncewicz, G. Dubin and J. M. Dąbrowski, *Catal. Today*, 2019, **335**, 538–549.
34 Y. Yang, F. An, Z. Liu, X. Zhang, M. Zhou, W. Li, X. Hao, C. S. Lee and X. Zhang, *Biomaterials*, 2012, **33**, 7803–7809.
35 B. O'Regan and M. Grätzel, *Nature*, 1991, **353**, 737–740.
36 J. Qin, J. Huo, P. Zhang, J. Zeng, T. Wang and H. Zeng, *Nanoscale*, 2016, **8**, 2249–2259.
37 M. Stylidi, D. I. Kondarides and X. E. Verykios, *Appl. Catal., B*, 2004, **47**, 189–201.
38 X. Zhang, L. Yu, C. Zhuang, T. Peng, R. Li and X. Li, *RSC Adv.*, 2013, **3**, 14363–14370.
39 W. Wu, F. Guo, J. Li, J. He and J. Hua, *Synth. Met.*, 2010, **160**, 1008–1014.
40 B. Wang, G. Y. Cui, B. B. Zhang, Z. Li, H. X. Ma, W. Wang, F. Y. Zhang and X. X. Ma, *Opt. Mater.*, 2020, **109**, 110202.
41 R. E. El-Mekawy and A. A. Fadda, *RSC Adv.*, 2017, **7**, 54706–54716.
42 R. E. El-Mekawy and A. A. Fadda, *Bioorg. Med. Chem. Lett.*, 2018, **28**, 1747–1752.
43 S. Naghibi and M. Gharagozlou, *J. Chin. Chem. Soc.*, 2017, **64**, 640–650.
44 M. Y. Rizal, R. Saleh, S. P. Prakoso, A. Taufik and S. Yin, *Mater. Sci. Semicond. Process.*, 2021, **121**, 105371.
45 D. A. Giannakoudakis, D. Łomot and J. C. Colmenares, *Green Chem.*, 2020, **22**, 4896–4905.
46 A. Singh and A. S. K. Sinha, *J. Energy Chem.*, 2018, **27**, 1183–1188.
47 L. S. Almazroai and R. E. El-Mekawy, *RSC Adv.*, 2019, **9**, 24670–24681.
48 Z. Lian, W. Wang, S. Xiao, X. Li, Y. Cui, D. Zhang, G. Li and H. Li, *Sci. Rep.*, 2015, **5**, 1–11.
49 E. Albiter, M. A. Valenzuela, S. Alfaro, G. Valverde-Aguilar and F. M. Martínez-Pallares, *J. Saudi Chem. Soc.*, 2015, **19**, 563–573.
50 P. Van Viet, B. T. Phan, D. Mott, S. Maenosono, T. T. Sang, C. M. Thi and L. Van Hieu, *J. Photochem. Photobiol., A*, 2018, **352**, 106–112.
51 A. Nagy and G. Mestl, *Appl. Catal., A*, 1999, **188**, 337–353.
52 R. E. El-Mekawy and R. S. Jassas, *Medchemcomm*, 2017, **8**, 897–906.
53 R. E. El-Mekawy, H. A. Elhady and H. F. Al-Shareef, *Polym. Polym. Compos.*, 2020, **29**, 563–573.
54 D. Gogoi, A. Namdeo, A. K. Golder and N. R. Peela, *Int. J. Hydrogen Energy*, 2020, **45**, 2729–2744.
55 L. M. Santos, W. A. Machado, M. D. França, K. A. Borges, R. M. Paniago, A. O. T. Patrocinio and A. E. H. Machado, *RSC Adv.*, 2015, **5**, 103752–103759.
56 T. Ali, A. Ahmed, U. Alam, I. Uddin, P. Tripathi and M. Muneer, *Mater. Chem. Phys.*, 2018, **212**, 325–335.
57 T. Munir, M. Sharif, H. Ali, M. Kashif, A. Sohail and N. Sabir, *Dig. J. Nanomater. Biostructures*, 2019, **14**, 279–284.
58 A. Litke, Y. Su, I. Tranca, T. Weber, E. J. M. Hensen and J. P. Hofmann, *J. Phys. Chem. C*, 2017, **121**(13), 7514–7524.
59 L. Mino, C. Negri, R. Santalucia, G. Cerrato, G. Spoto and G. Martra, *Molecules*, 2020, **25**(20), 4605.
60 B. Kumar, K. Smita, Y. Angulo and L. Cumbal, *Green Process. Synth.*, 2016, 371–377.
61 A. Mohagheghian, S. Karimi, J. Yang and M. Shirzad-siboni, *J. Adv. Oxid. Technol.*, 2015, **18**(1), 61–68.
62 N. Manwar, A. Chilkalwar, K. K. Nanda, Y. S. Chaudhary, J. Subrt, S. S. Rayalu and N. K. Labhsetwar, *ACS Sustainable Chem. Eng.*, 2016, **4**, 2323–2332.
63 Z. Chen, X. Jiang, C. Zhu and C. Shi, *Appl. Catal., B*, 2016, **199**, 241–251.
64 M. Wang, S. Shen, L. Li, Z. Tang and J. Yang, *J. Mater. Sci.*, 2017, **52**, 5155–5164.
65 F. Guzman, S. S. C. Chuang and C. Yang, *Ind. Eng. Chem. Res.*, 2013, **52**, 61–65.
66 K. Han, W. Li, C. Ren, H. Li, X. Liu, X. Li, X. Ma, H. Liu and A. Khan, *J. Taiwan Inst. Chem. Eng.*, 2020, **112**, 4–14.
67 D. P. Kumar, N. L. Reddy, M. Karthik, B. Neppolian, J. Madhavan and M. V. Shankar, *Sol. Energy Mater. Sol. Cells*, 2016, **154**, 78–87.
68 A. Tiwari and U. Pal, *Int. J. Hydrogen Energy*, 2015, **40**, 9069–9079.
69 D. Popugaeva, T. Tian and A. K. Ray, *Int. J. Hydrogen Energy*, 2020, **45**, 11097–11107.
70 W. Ghann, H. Kang, E. Emerson, J. Oh, T. Chavez-Gil, F. Nesbitt, R. Williams and J. Uddin, *Inorg. Chim. Acta*, 2017, **467**, 123–131.
71 M. Guo, P. Diao, Y.-J. Ren, F. Meng, H. Tian and S.-M. Cai, *Sol. Energy Mater. Sol. Cells*, 2005, **88**, 23–35.
72 X. Zhang, X. Zhang, K. Feng, X. Hu, J. Fan and E. Liu, *RSC Adv.*, 2021, **11**, 11872–11881.

73 B. Zhang, X. Hu, E. Liu and J. Fan, *Chin. J. Catal.*, 2021, **42**, 1519–1529.
74 K. Mohammadi, A. Moshaii, M. Azimzadehirani and Z. S. Pourbakhsh, *J. Mater. Sci.: Mater. Electron.*, 2019, **30**, 1878–1884.
75 M. Ni, D. Y. C. Leung, M. K. H. Leung and K. Sumathy, *Fuel Process. Technol.*, 2006, **87**, 461–472.
76 G. Y. Yao, Q. L. Liu and Z. Y. Zhao, *Catalysts*, 2018, **8**(6), 236.
77 J. Joo, Y. Ye, D. Kim, J. Lee and S. Jeon, *Mater. Lett.*, 2013, **93**, 141–144.
78 K.-Y. A. Lin and Z.-Y. Zhang, *Chem. Eng. J.*, 2017, **313**, 1320–1327.